

# X-ray computed tomography of peat soils: measuring gas content and peat structure

Nicholas Kettridge\* and Andrew Binley

Lancaster Environment Centre, Lancaster University, Lancaster LA1 4YQ UK

## Abstract:

The potential of using X-ray computed tomography (CT) to (i) analyse individual biogenic gas bubbles entrapped within peats and (ii) produce reliable descriptors of peat structure is examined. Existing approaches used to study biogenic gas bubbles measure the gas content of volumes of peat many orders of magnitude larger than most bubbles, and are, therefore, of little use in helping to understand bubble dynamics. In many peatland studies, the description of peat structures is derived from only a few relatively basic metrics; principally the porosity, the bulk density, and the von Post humification scale. CT is applied to identify and quantitatively analyse the size, location and shape of individual gas bubbles entrapped during the saturation of a 200 cm<sup>3</sup> sample of *S. fuscum*. 3421 gas bubbles were identified, ranging in size from 0.1 mm<sup>3</sup> to 99.9 mm<sup>3</sup>. These gas bubbles were non-randomly distributed, clustered predominantly in the vertical plane. When analysing the peat structure, *Sphagnum* peat and water are shown to be indistinguishable within CT scans. Peat samples were therefore prepared prior to scanning by flushing the peat with lead (II) nitrate solution to increase the linear attenuation of the *Sphagnum*. *Sphagnum* stems and branches were analysed, producing metrics of the peat structure; including stem and branch lengths, radii and orientation. In a 100 cm<sup>3</sup> sample of *S. magellanicum*, the length of all *Sphagnum* stems totalled 1.82 m, with an average radius of 0.65 mm. The *Sphagnum* stems and branches were both preferentially orientated in the horizontal direction. Copyright © 2008 John Wiley & Sons, Ltd.

*Additional supporting information may be found in the online version of this article.*

KEY WORDS X-ray computed tomography; peatland; gas bubbles; peat structure

Received 18 December 2007; Accepted 23 May 2008

## INTRODUCTION

Northern peatlands may be defined as peatlands north of 45°N. They occupy large areas in Russia, Canada, the USA, Finland and Sweden, and may vary in thickness from a few decimetres to 10 or more metres. They are an important component of the global carbon cycle, containing at least one-third of the global soil carbon pool (Maltby and Proctor, 1996), and are often of high conservation value because of their unique vegetation, and to a lesser extent faunal, assemblages (Rydin and Jeglum, 2006). Much current work on peatlands is concerned with their role as sources of atmospheric methane and their ecohydrological functioning (Strack *et al.*, 2005). Both areas of research require an understanding of the sub-surface processes in the peat. For example, recent work has suggested that a significant proportion (>40%) of methane lost from peatlands does so as bubbles (Tokida *et al.*, 2007)—the methane is produced by anaerobic decay of peat and may be in both dissolved and free-phase (bubble) form. However, an understanding of how and where methane-containing bubbles build up in the peat, how the bubbles move to the peatland surface, and how the structural properties of the peat affect bubble

buildup and movement is still very limited (Kellner *et al.*, 2006). In large part this lack of understanding is the result of an inability to scan or record the size, shape and disposition of bubbles within the peat. Existing methods such as time domain reflectometry simply give the gas content of volumes of peat many orders of magnitude larger than most bubbles, and are, therefore, of little use in helping us understand bubble dynamics (Kellner *et al.*, 2006; Baird *et al.*, 2004).

Although much interest in methane-containing bubbles relates to the bubbles as conveyors of methane to the peatland surface, it has also been shown that bubble accumulations can affect peat hydraulic conductivity (Beckwith and Baird, 2001; Baird and Waldron, 2003), hydraulic gradients within the peat (Rosenberry *et al.*, 2003; Glaser *et al.*, 2004), peatland surface elevation (Stack *et al.*, 2005) and peat water storage properties (Kellner *et al.*, 2005). Through these effects, it has been suggested that bubbles affect the biogeochemical functioning of peatlands (Strack *et al.*, 2006), thus providing a further rationale for the need to understand bubble dynamics.

The structure of peat varies spatially within a peatland. Vertically down through the peat profile, the peat generally becomes more decomposed, from living *Sphagnum* at the peat surface through to well-decomposed peat with no definable *Sphagnum* remains at depth (Ingram, 1978). These spatial variations in the decomposition

\* Correspondence to: Nicholas Kettridge, Lancaster Environment Centre, Lancaster University, Lancaster LA1 4YQ UK.  
E-mail: N.Kettridge@lancaster.ac.uk

of the organic matter can be either gradual or abrupt. The most widely identified change in peat structure is between the acrotelm and the catotelm. The former is the upper 0.05–0.5 m and consists of the growing surface and relatively poorly-decomposed plant remains. Its lower limit is defined as the lowest position of the water table (i.e. greatest distance from the ground surface) during a drought year. Below it is the catotelm which is anoxic and contains generally well-decomposed peat (Daulat and Clymo, 1998). Superimposed on this vertical decomposition profile are horizontal variations in the peat structure resulting from variations in near-surface wetness and plant species composition across the peatland surface. Spatial variations in the water-table depth and vegetation types of different peatland microhabitats produce variations in the level of decomposition prior to the peat becoming part of the catotelm as the peatland grows. Because these different peat types have different hydraulic conductivities and because they are preserved in the peat as the peatland grows they can have a profound effect on the ecohydrological 'behaviour' of the bog for many hundreds of years after they were laid down (Belyea and Baird, 2006). To understand how such patterns affect water, gas and solute movement through a peat deposit it is necessary to be able to describe the key structural variations between different peat types.

In many peatland studies only a few relatively basic metrics are used to describe the structure of peat; principally the porosity, the bulk density, and the degree of peat humification using the von Post humification scale (Kellner *et al.*, 2005). Unfortunately, beyond basic description, these provide little information on the ability of the peat to trap, store and conduct water and gases (Price *et al.*, 2005) and are prone to errors in measurement caused by damage to the peat sample during preparation for a measurement—many peat samples for porosity and bulk density measurement are cut from larger cores at intervals of a few centimetres, resulting in a high ratio of damaged (cut) surface area to volume. Finally, it is worth noting that the von Post humification scale is categorical and sometimes difficult to apply (different workers often arrive at a different humification score for the same peat sample). Thus, although it grades peat humification on a scale of 1–10 (with 1 the least humified), the implied increase in degree of humification between, say a score of 2 and a score of 1, is not the same as between a score of, say, 8, and one of 7.

It is clear from the above that there is a need for more reliable descriptors of peat structure. The purpose of the work described in this paper was to test the potential utility of one new method—X-ray computed tomography (CT)—as the basis of such a reliable description. X-ray CT is a 3D, high-resolution, non-destructive visualisation technique. Originally developed for the medical industry, the cost of CT scanners has reduced substantially in recent years making them available to environmental scientists. In peatland science, the approach has only previously been applied to the measurement of peat moisture contents under varying suctions (Blais, 2005).

However, X-ray CT has the potential to provide a wealth of information for peatland studies. The aim of this article is to identify the potential of the CT approach for the measurement of entrapped gas bubbles within *Sphagnum* peat and the characterisation of different peat types. The CT approach is first outlined, and then the potential of the approach for measuring entrapped gas bubbles and characterising peat structure is assessed.

## X-RAY COMPUTED TOMOGRAPHY

There are a number of general reviews on the application of CT within environmental science (Ketcham and Carlson, 2001; Wildenschild *et al.* 2002); hence, only a brief overview of the CT approach is provided here. As X-rays pass through a material they are attenuated; the X-ray intensity is reduced. This attenuation ( $\mu$ ) is dependent on the density of the material, its atomic number and the energy of the X-rays. For a monochromatic X-ray energy source, the X-ray intensity ( $I$ ) leaving a material is given by:

$$I = I_0 e^{-\mu x} \quad (1)$$

where  $I_0$  is the original X-ray intensity and  $x$  (m) is the pathlength of the X-rays through the material. A conical CT scanner, for example the X-TEK Benchtop CT160Xi ([www.xtekxray.com](http://www.xtekxray.com)), used in this study (with a dual field image intensifier coupled to a 12 bit digital charged couple device (CCD)), takes an averaged 2D digital X-ray image of the sample (a radiograph). This X-ray image is composed of over a million pixels, with each pixel value equal to  $I$  for given parallel pathlengths through the sample. The conical CT scanner obtains such 2D X-ray images at different angles around an axis of rotation. A 3D image of the sample (related to the linear attenuation of the material) is produced by combining the information within each of these 2D X-ray images. The 3D image is constructed by successively overlaying the average attenuations of each X-ray path over a square grid while applying a filter to reduce image noise. Where X-ray paths with a higher attenuation intersect, the attenuation of the reconstructed image is increased. Where the higher attenuations do not intersect, the error is removed by the filter. The values of the grey scale image that is produced are linearly related to the linear attenuation of the material. However, the absolute values are arbitrary. Therefore, these values are often calibrated to a known scale. In this study, the reconstructed images have been scaled to the linear attenuation (air = 0.0, water = 17.1 m<sup>-1</sup> at 100 keV).

CT scanners are designed for specific applications and thus the maximum size of the sample that can be scanned, the resolution of the CT image, and the scan time vary substantially. The largest volume that can be imaged within a single scan by the X-TEK Benchtop CT160Xi is 72 mm in diameter and 72 mm in height. Although the height of the sample that can fit within the scanner can reach up to 700 mm, the 72 mm high image can

only be obtained from within the bottom 140 mm of any sample. This maximum sample size can be imaged at a resolution of approximately 100  $\mu\text{m}$ . Scan times vary between 30 min and 2 h depending on the number and quality of the radiographs obtained.

### SAMPLE COLLECTION

In order to test the potential utility of X-ray CT for measuring bubbles and peat structural properties, a sample of *S. fuscum* peat and two samples of *S. magellanicum* peat (with surface areas of 0.0150  $\text{m}^2$ , from the peat surface to a depth of 0.13 m) were collected from a blanket bog in the Flow Country, Scotland, while a sample of *S. pulchrum* peat (with surface areas of 0.0033  $\text{m}^2$ , from the peat surface to a depth of 0.13 m) was collected from Cors Fochno, a raised bog in Wales. Large areas of both sites are undisturbed and provide a good representation of many northern peatlands. Each sample was frozen soon after collection, then defrosted prior to use. Once defrosted, the samples were trimmed with scissors to the specific dimensions of the cylindrical sample holders used to hold the peat sample during the CT scans (dimensions provided below for each scan). All scans were performed in the centre of the extracted core, with the centre of the 72 mm image at a depth of 75 mm below the peat surface. This measurement was selected to examine the entrapment of biogenic gas bubbles and peat structure close to the peat surface. The hydrology of northern peatlands is very sensitive to the zone of poorly decomposed near surface peat, with hydraulic conductivities generally orders of magnitude greater than those deeper within the peat profile (Ingram, 1978). Therefore, it is within this near surface zone that entrapped gas bubbles, and the associated affect on the hydraulic conductivity (Baird and Waldron, 2003), may have a significant influence on peatland hydrology.

As far as the authors are aware, only Blais (2005) has previously applied the CT approach to scan poorly decomposed peat. A range of peat types was used to identify any apparent difficulties in applying the approach to image different poorly decomposed *Sphagnum* peat. Peat types were then arbitrarily selected to analysis either the entrapped biogenic gas content or the peat structure. The *S. fuscum* sample was used to analyse the spatial distribution of entrapped gas bubbles. The samples of *S. magellanicum* and *S. pulchrum* were used to identify the structure of the peat. The details of the CT scan, sample sizes and any additional preparation of the sample prior to scanning are presented prior to the presentation of the CT images and the subsequent data analysis.

### ANALYSIS OF ENTRAPPED GAS BUBBLES

The number, size, shape and location of entrapped gas bubbles in the *S. fuscum* peat were measured. Combined with measurements of peat structure, these metrics can be used to identify the characteristics of the peat responsible

for gas bubble entrapment. These metrics also enable the threshold gas content, beyond which bubbles start to move upwards through the peat profile (Kellner *et al.*, 2006), to be analysed. Although previous studies have suggested the existence of such a threshold (Baird *et al.*, 2004), it is unknown how a threshold relates to the forces acting on *individual* gas bubbles—the threshold approach has been developed with bulk bubble content data obtained from TDR measurements. Small-scale measurements of bubble sizes, shapes and locations can be used to characterise the growth and movement of individual gas bubbles and identify how bubble loss may be represented by a bulk threshold gas content.

Bubbles in peat may form from the methane produced by anaerobic decay of peat (see 'Introduction'). As shown by Baird and Waldron (2003), bubbles may also be trapped by a rising water table and then act as foci for bubble growth as methane is produced. Rather than incubate the *S. fuscum* peat sample (diameter 0.06 m, depth 0.13 m) and wait for biogenic gas bubbles to form, it was saturated slowly from its base with distilled water and used immediately. This means that it contained encapsulated air only; however, it was decided that there should be sufficient bubbles in the sample to test the utility of X-ray CT for bubble measurement. After wetting, the sample was scanned (voltage 130 keV, current 184  $\mu\text{A}$ ) using a 0.5 mm copper filter to remove X-rays below 60 keV. 1,541 radiographs of the sample were obtained around the axis of rotation, with each radiograph stacked 32 times to reduce image noise. The reconstructed 3-D volume was cropped to isolate the *Sphagnum* sample; removing the sample holder and the region where the entrapment of gas bubbles may be significantly influenced by the boundary between the sample holder and the peat. This produced a volume composed of  $2.3 \times 10^8$  voxels, each  $100 \times 100 \times 100 \mu\text{m}$ . Because of small errors in the measured radiographs and limitations in the reconstruction process, the measured linear attenuation of voxels composed of only one constituent of the peat sample (e.g. air, water) are not represented by a single linear attenuation, but by a range of attenuations, approximating a normal distribution. The reconstructed image of the *S. fuscum* sample shows two such normal distributions (Figure 1). The peak at a linear attenuation of  $14.8 \text{ m}^{-1}$  is associated with voxels composed entirely of water and/or *Sphagnum*. The similarity of the linear attenuations of water and saturated *Sphagnum* means it is impossible to differentiate between these two constituents in an unprepared sample (Blais, 2005). This problem is discussed later under 'Analysis of peat structure'. Until then, for simplicity, this peak is defined as the water peak. The smaller peak at a linear attenuation of  $1.5 \text{ m}^{-1}$  is associated with voxels composed entirely of air trapped during the wetting of the sample (Beckwith and Baird, 2001; Baird and Waldron, 2003). Voxels located at the interface between the gas bubbles and water have a linear attenuation between that of the air and water. The linear attenuation of these voxels are an artefact of the reconstruction process, which

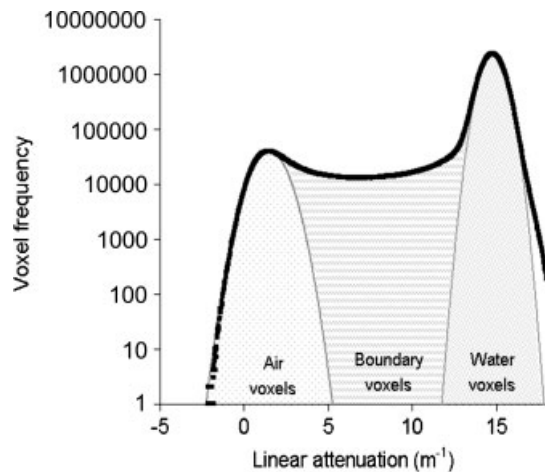


Figure 1. Histogram of the linear attenuation of all voxels in the reconstructed image of *S. fuscum* (black squares). Number of voxels calculated as being composed of air, water and boundary voxels are marked

smooths the air–water boundary (Clausnitzer and Hopmans, 2000).

#### Bulk measurement of gas content

The bulk gas content of the peat was measured by assuming that the linear attenuation distribution is bimodal; consisting of two normal distributions representing voxels composed only of air and water, respectively. The fitting of normal distributions to the air and water peaks allows the number of voxels composed entirely of air and water to be calculated. Voxels in addition to these two normal distributions, at linear attenuations greater than the air peak, and less than the water peak, are assumed to be composed of both air and water. The proportion of each voxel composed of a mixture of air and water can be calculated from the equation of the bulk linear attenuation of a volume composed of two immiscible phases (Vinegar and Wellington, 1987):

$$\mu_{mix} = \mu_1 \left( \frac{V_1}{V_{mix}} \right) + \mu_2 \left( \frac{V_2}{V_{mix}} \right) \quad (2)$$

where  $V$  is the volume, and subscripts 1, 2 and  $mix$  denote phase 1, phase 2 and the mixture, respectively. The bulk volumetric gas content ( $\theta$ ) is then equal to:

$$\theta = \frac{N_{caf} + \sum_{n=1}^{N_{paf}} \theta_i}{N_{total}} \cdot 100 \quad (3)$$

where  $\theta_i$  is the proportion of each voxel between the two normal distributions composed of air (equal to  $V_1/V_{mix}$  in Equation (2)),  $N$  is the number of voxels and subscripts  $caf$ ,  $paf$  and  $total$  denote completely air filled, partly air filled and all voxels, respectively.

A normal distribution function was fitted to the rising limb of the air peak, minimising the root mean squared error (RMSE) between voxel frequencies (Figure 1). This process was repeated for the falling limb of the water peak. The bulk gas content was calculated from

Equation (2), assuming that the linear attenuation of water equals  $14.8 \text{ m}^{-1}$ , and that the linear attenuation of air equals  $1.5 \text{ m}^{-1}$ . This gives a measured bulk volumetric gas content of 4.8% for the *S. fuscum* sample. This value matched closely with the gas bubble content of 6.8% ( $n = 36$ , st. dev = 0.035) measured previously with TDR probes in samples of *S. magellanicum*, *S. papillosum*, *S. pulchrum* and *S. cuspidatum* by Beckwith and Baird (2001), Baird and Waldron (2003) and Baird *et al.* (2004).

The approach described above is considered to provide an accurate estimation of the bulk gas content of the peat. However, it makes detailed analysis of the spatial nature of the entrapped gas bubbles difficult because it is impossible to identify the volumetric gas content of each individual voxel. Therefore, a simple threshold approach was also applied, classifying each voxel as either air or water. A threshold linear attenuation of  $8.15 \text{ m}^{-1}$ , equivalent to a 50% gas content (Equation (2)), produced a bulk gas content of 4.35%. This gas content is not dissimilar to the 4.8% identified above. A 3D representation of the classified image is presented in Figure 2. Voxels classified as water are transparent, while voxels classified as air are represented by a grey scale which relates to the linear attenuation of the voxel. These images were analysed to provide quantitative information on bubble numbers, sizes, locations and shapes.

#### Bubble numbers and size

Each individual bubble was identified by grouping together neighbouring voxels that were classified as gas into a single 'particle'. The volume of each bubble was calculated by summing together the number of voxels that were grouped. 5285 gas bubbles were identified in the sample of *S. fuscum*, ranging in size from one voxel ( $0.001 \text{ mm}^3$ ) to 99 922 voxels ( $99.922 \text{ mm}^3$ ). 50% of the gas content was composed of 216 individual gas bubbles (Figure 3), while 198 gas bubbles were only one voxel in size. Due to the threshold value applied, a proportion of these smaller bubbles is likely to consist of voxels of water, with a low measured linear attenuation, being erroneously classified as gas. Although this is impossible to validate, it appears reasonable to assume a minimum gas bubble size, below which the identified gas bubbles are assumed insignificant. A threshold of 100 voxels has been applied here, equivalent to a bubble size of  $0.1 \text{ mm}^3$ . Although 1,864 bubbles were discarded by this threshold, they accounted for only 0.5% of the total gas volume.

#### Bubble locations

The CT image was analysed to identify whether the entrapped gas bubbles were located randomly within the sample of *S. fuscum*. If the entrapped gas bubbles are non-randomly distributed, it suggests that the structural properties of the peat that entrap air during saturation vary spatially within the sample. An analysis of peat metrics (see 'Analysis of peat structure') could then be used to

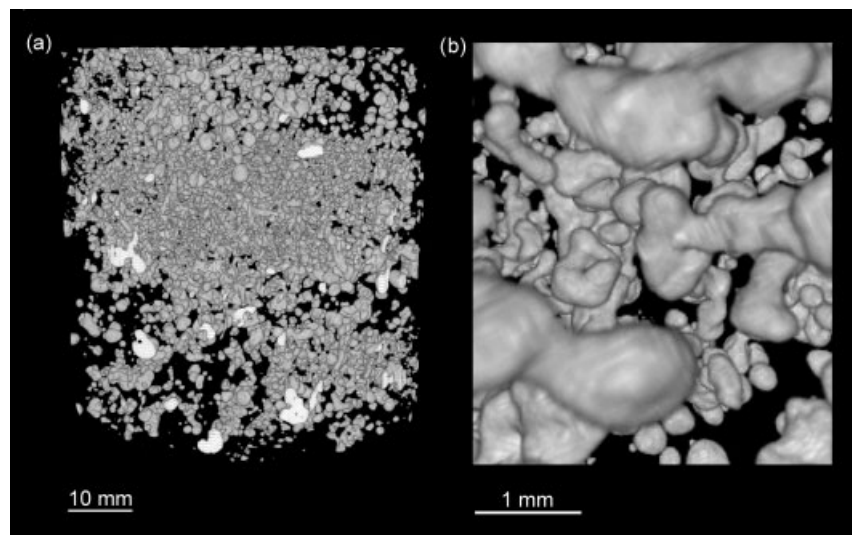


Figure 2. 3D image of gas bubbles within (a) the entire sample and (b) a small section of the sample of *S. fuscum*. Voxels classified as water are transparent, while voxels classified as air are represented by a grey scale which relates to the linear attenuation of the voxel

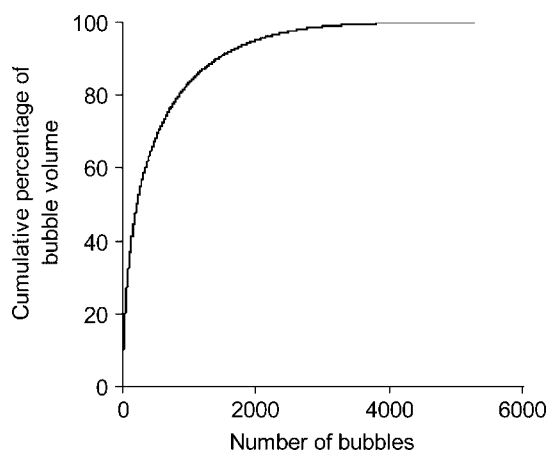


Figure 3. Cumulative percentage of bubble volume by number of bubbles (ordered from largest to smallest bubbles) within the sample of *S. fuscum*. Gas bubbles identified using ImageJ 3D Object counter, applying a linear threshold of  $8.15 \text{ m}^{-1}$  to classify the sample as either gas or water and *Sphagnum*

identify the structural attribute responsible for this spatial variability.

To reduce computer resources, the image resolution was decreased in the horizontal plane by 50% and cropped to produce a rectangle 45 mm by 48 mm. Each gas bubble was identified, grouping neighbouring voxels, which were classified as gas (as above) using ImageJ 3D Object counter (<http://rsbweb.nih.gov/ij>). ImageJ 3D Object counter identifies the mass centre of each gas bubble, in addition to the bubble volume. Bubbles less than  $0.1 \text{ mm}^3$  were excluded from the subsequent data analysis, in accordance with the threshold identified above.

Gas bubble locations cannot be treated as point measurements. The minimum distance between a gas bubble and its nearest neighbour depends on the size of the bubble itself, and the size of those bubbles surrounding it. Analysis of spatial randomness from nearest neighbour measurements (Hopkins and Skellam, 1954) is therefore

not applicable. Instead, a 3D quadrature approach (Greig-Smith, 1952) was applied. The sample was divided into 96 equal quadrates and the number of bubbles contained within each quadrate was calculated. If the entrapped gas bubbles are randomly distributed within the sample of peat, the relative variance (equal to the variance of the number of bubbles within each quadrate divided by the mean number of bubbles within each quadrate) will be equal to one (Clapham, 1936). For clustered samples, the relative variance is greater than unity and for uniform samples it is less than unity. The significance of the deviation of the relative variance from unity is calculated from a 't-test', giving the probability,  $P$ , of obtaining the observed distribution of bubbles by chance. Although this approach also assumes point measurements, by applying quadrates approximately  $5 \times 5 \times 5 \text{ mm}$  in size (seven orders of magnitude larger than the largest bubble), it is assumed that the effects of varying gas bubble size should be kept to a minimum. Edge effects were removed from the data analysis by excluding the region 2 mm from the edge of the cropped image; equal to the maximum bubble radius (calculated from the maximum bubble volume, assuming a spherical bubble). The zone at the edge of the cropped image was removed from the analysis because gas bubbles with their centres of mass outside the cropped volume, but which encroach inside the sampling volume, will be identified in this analysis as smaller gas bubbles with their centres of mass clustered at the edge of the cropped image.

The entrapped gas bubbles are clustered, with a relative variance of 3.9 ( $P < 0.0005$ ). While the location of the bubbles is non-random in 3D, the axes in which the bubbles are clustered have not been identified. These axes were assessed by comparing bubble locations using a single line of 100 quadrates in each plane. The bubble locations were clustered in the  $x$  and  $y$  planes, with a relative variance of 1.5 ( $P < 0.0005$ ) and 2.0 ( $P < 0.0005$ ), respectively. In the  $z$  plane, the relative

variance increased to 5.1 ( $P < 0.0005$ ). This signifies a clear bias in the clustering of the gas bubbles in the vertical plane (Figure 4a) compared with the horizontal plane (Figure 4b). At the base and at the surface of the sample, bubble numbers are far fewer than at a height of 40 mm from the base of the sample. This suggests that vertical variations exist in the structure of the sample of *S. fuscum* which produce the zone of preferential gas entrapment.

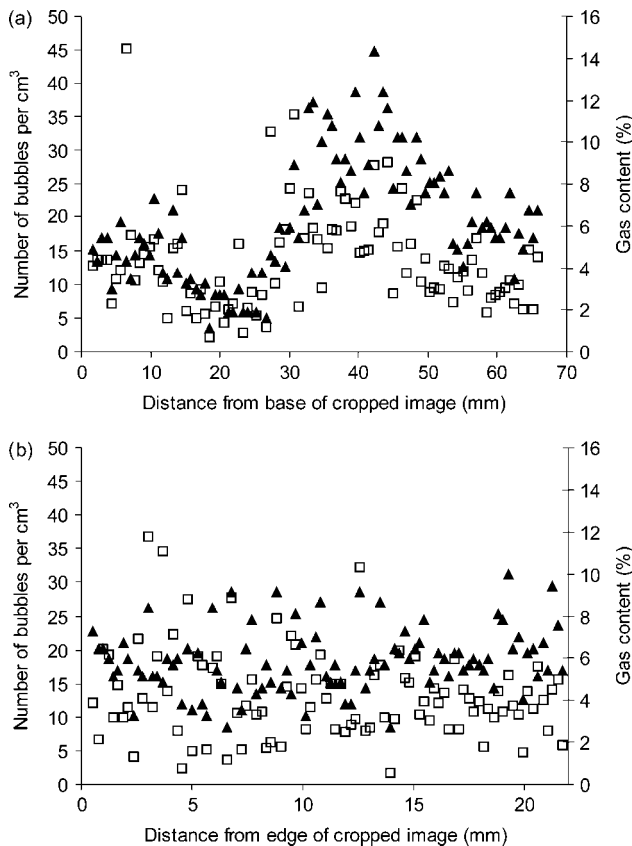


Figure 4. The spatial variation in density of gas bubbles (triangles) and the entrapped gas content (squares) in (a) the vertical and (b) the horizontal plane within the cropped image of the sample of *S. fuscum*. The number of bubbles with their centre of mass within each of the one hundred  $366 \text{ mm}^3$  (a) vertical or (b) horizontal slices through the sample are summed and divided by the volume of the slice to calculate the density and gas content, respectively

### Bubble shape

The circularity,  $C$ , of a 2D shape is given by:

$$C = \frac{4\pi A}{P^2} \quad (4)$$

where  $A$  ( $\text{mm}^2$ ) is the area of a 2D slice through the bubble and  $P$  (mm) is the bubble perimeter.  $C$  ranges from one for a circle to zero for a straight line. Using the measurement command within ImageJ,  $C$  was calculated for the bubbles that were identified in each 2D vertical and horizontal slice through the reconstructed 3D image. These bubbles were identified by grouping neighbouring voxels that were classified as gas within each 2D slice. Therefore, for each 3D bubble, multiple measurements of  $C$  were obtained. When  $A$  of a slice through a bubble was less than 20 pixels, errors in the measurement of  $P$  by the ImageJ measurement command are considered to be significant, producing erroneous measurements of  $C$ . Therefore, such bubbles have been removed from subsequent analysis.

The circularity of the bubbles decreases with increasing  $A$ , and is best approximated by log linear relationship (Figure 5):

$$C = m \ln(A) + c \quad (5)$$

where  $m$  and  $c$  are constants equal to  $-0.112$  and  $0.797$ , respectively, in the horizontal plane ( $R^2 = 0.36$ ; Figure 5a). Smaller bubbles are more spherical because they can be contained within individual pores. The circularity of the bubbles is slightly anisotropic. In the vertical direction, bubbles are significantly more circular than in the horizontal direction (the intercept of the relationship between  $C$  and  $A$  differs significantly ( $P < 0.001$ ) between the horizontal and vertical planes). However, although significant, the difference in the intercepts is small, equal to only 0.005.

### ANALYSIS OF PEAT STRUCTURE

It was noted above that voxels containing *Sphagnum* remains cannot be identified because their linear attenuations are indistinguishable from water. *Sphagnum* is composed predominantly of water filled hyaline cells.

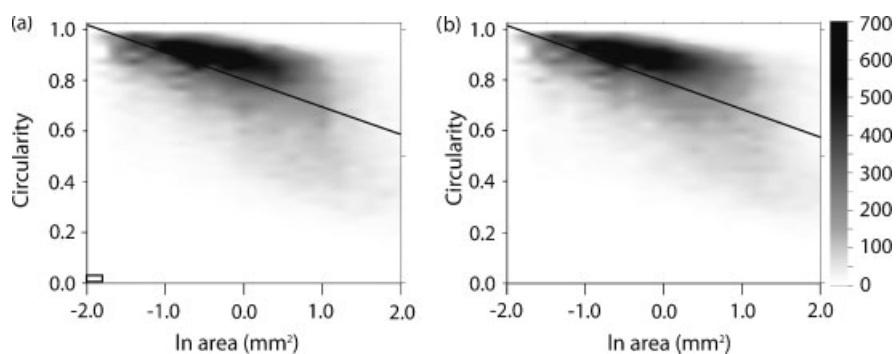


Figure 5. Circularity of entrapped gas bubbles measured in the a) horizontal and b) vertical planes within the sample of *S. fuscum*. Grey scale represents the density of points per unit area (represented by rectangle at bottom left of (a)). Lines represent linear regression

The bulk linear attenuation of *Sphagnum* remains therefore differ little from the pore water. Consequently, to identify the structure of the peat it is necessary to apply dual energy CT or to prepare the sample prior to scanning, either to alter the linear attenuation of the pore fluid or of the *Sphagnum*.

#### Dual energy CT

The linear attenuation of a material varies with the energy of the X-rays. As the X-ray energy increases, the linear attenuation of a material generally declines. If the linear attenuations of two materials are indistinguishable at a single X-ray energy, they may be identified by calculating the change in linear attenuation between two different energies (assuming the gradient of the relationship between X-ray energy and linear attenuation differ for the two materials). This approach was applied in an attempt to distinguish between the water content and the *Sphagnum* peat. Two CT scans were performed on the sample of *S. pulchrum* (diameter 0.6 m, height 0.6 m), at 60 keV and 130 keV, and at 330 and 100  $\mu\text{A}$ , respectively. 1,567 images were obtained around the centre of rotation; each image stacked 32 times to reduce image noise. The ratio of the linear attenuation of *Sphagnum* at the different energies varied indistinguishably from the ratio of the water. Initial investigations, therefore, suggest that this approach is unable to differentiate between the *Sphagnum* and pore water.

#### Alteration of the linear attenuation of the pore fluid

A sample of *S. magellanicum* (diameter 0.05 m, height 0.05 m) was saturated slowly from its base with water and then flushed with a solution of potassium bromide (KBr; 100% concentration). The KBr solution increased the linear attenuation of the pore fluid by two orders of magnitude (comparable with the difference in linear attenuation between air and water). Bromide has been shown to be a conservative tracer in peat soils (Gafini, 1986). Sorption of KBr by *Sphagnum* is low, maximising the differentiation between the linear attenuation of the peat and the pore water. The first sample of *S. magellanicum* was scanned (130 keV, a current of 226  $\mu\text{A}$ ) using a 0.5 mm copper filter to remove X-rays less than approximately 60 keV. 1,239 images of the sample were obtained around the axis of rotation; each image stacked 32 times to reduce image noise. This approach of visualising the *Sphagnum* proved unsuccessful. First, it proved difficult to maintain a uniform pore water concentration of KBr within the sample. Variations in the linear attenuation of the pore fluid were more substantial than variations between the *Sphagnum* and the pore water. Secondly, the increased linear attenuation of the sample substantially reduced the measured values of  $I$  (Equation (1)), making variations across the sample difficult to distinguish.

#### Alteration of the linear attenuation of *Sphagnum*

The peat structure may be visualised by increasing the linear attenuation of the *Sphagnum* remains. Peat

has a significant sorption capacity for lead ions (Ho and McKay, 1999). Because the linear attenuation of the lead (II) nitrate solution (50% concentration) is five times that of water, the sorption of lead ions will significantly increase the linear attenuation of the peat. Flushing a sample of peat with lead (II) nitrate solution may, therefore, enable the peat structure to be distinguished from the pore fluid.

The second sample of *S. magellanicum* (diameter 0.05 m, height 0.05 m) was saturated slowly from its base with water, flushed with a solution of lead (II) nitrate (50% concentration) and left for 24 h to allow full sorption. The sample was then flushed with water for an additional 24 h in order to remove the remaining lead (II) nitrate from the pore fluid. The prepared sample was scanned at a voltage of 60 keV and a current of 334  $\mu\text{A}$ . 1,213 2D X-ray images were obtained around an axis of rotation; each image was stacked 32 times to reduce image noise.

The water and air peaks are clearly identifiable at linear attenuations of 4.7  $\text{m}^{-1}$  and 28.3  $\text{m}^{-1}$ , respectively (Figure 6). A smaller peak is also evident at a linear attenuation of 49.7  $\text{m}^{-1}$ . This peak is associated with the *Sphagnum* stems and branches that sorbed the lead (II) nitrate. The *Sphagnum* branches are shown in Figure 7a, by observing voxels with a linear attenuation greater than 43.7  $\text{m}^{-1}$ . *Sphagnum* branches have a lower linear attenuation. They are visible in Figure 7b, with the *Sphagnum* stems, showing voxels with a linear attenuation greater than 33.8  $\text{m}^{-1}$ .

Even with the increased linear attenuation of the *Sphagnum* stems and branches, the *Sphagnum* leaves cannot be identified. *Sphagnum* leaves are composed predominantly of large water-filled hyaline cells, with a small proportion of chlorophyllose cells (Rydin and Jeglum, 2006). Even if the linear attenuations of the chlorophyllose cells are increased substantially, the average increase in the linear attenuation of the voxel is minimal, because the cells comprise such a small proportion of the total volume. Therefore, the visualisation

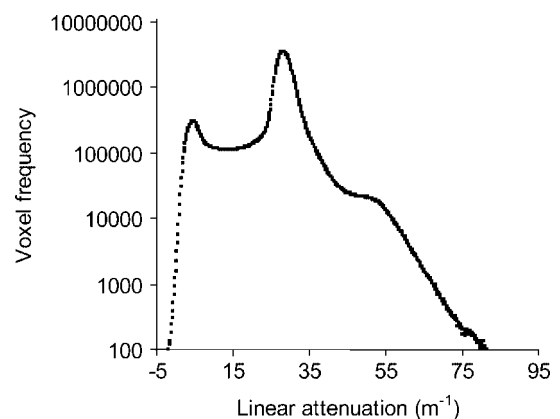


Figure 6. Histogram of the linear attenuation of all voxels in the reconstructed image of the sample of *S. magellanicum* after being flushed with a solution of lead (II) nitrate. The peaks at linear attenuations at 4.7, 28.3 and 49.7  $\text{m}^{-1}$  represent voxels composed of air, water and sorbed *Sphagnum*, respectively

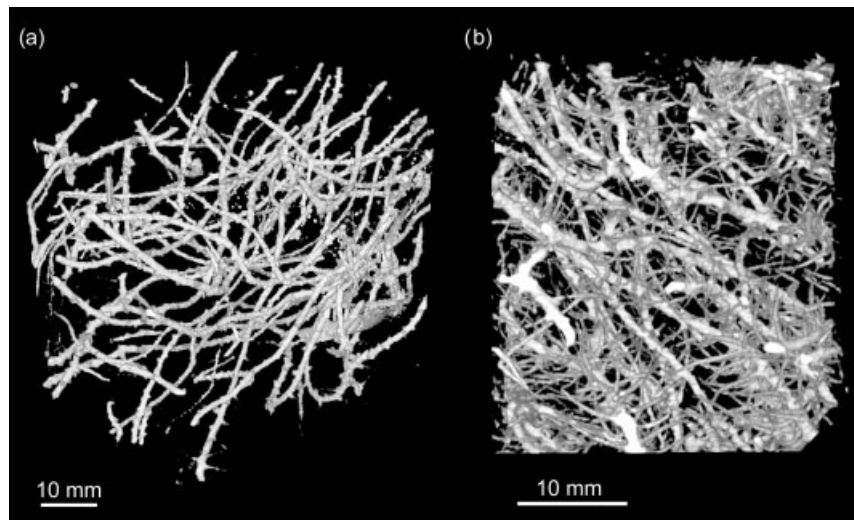


Figure 7. 3D representation of (a) *Sphagnum* stems and (b) *Sphagnum* stems and branches. Note the difference in scale between the images. Voxels classified as water or air, are transparent, while voxels classified as *Sphagnum* are represented by a grey scale which relates to the linear attenuation of the voxel

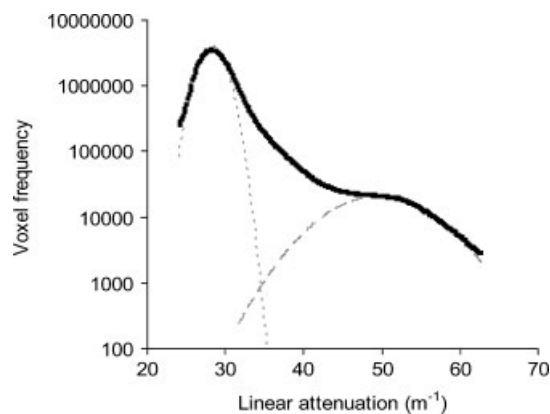


Figure 8. Histogram of the linear attenuation of all voxels in the reconstructed image of the second *S. magellanicum* sample after being flushed with a solution of lead (II) nitrate (black squares). The peaks at linear attenuations of 28.3 and 49.7  $\text{m}^{-1}$  represent voxels composed of water and sorbed *Sphagnum*, respectively. Voxels of a linear attenuation less than 24  $\text{m}^{-1}$  are excluded from the figure. The number of voxels calculated as being composed solely of water and sorbed *Sphagnum* are represented by the dotted grey line and dashed grey line, respectively

of the *Sphagnum* leaves appears an unrealistic goal with more widely available CT technology.

#### Measurement of porosity

Identification of the *Sphagnum* stems and branches enables the extraction of quantitative information about the peat structure. The bulk porosity of the sample was calculated by fitting normal distributions to the linear attenuation histogram (as above). Normal distributions were fitted to the rising limb of the water peak and the falling limb of the *Sphagnum* peak (Figure 8) by minimising the RMSE (the air peak was ignored when fitting these normal distribution). The bulk porosity calculated from Equations (2) and (3) equals 96.3%, and is similar to previous measurement of porosity presented for other samples of poorly decomposed near surface peat (Beckwith and Baird, 2001). However, this method does

not indicate whether an individual voxel is composed of water or *Sphagnum*, and so prevents any spatial analysis of the *Sphagnum* stems and branches.

A threshold linear attenuation was calculated by selecting the mid-point between the water and *Sphagnum* peaks (as in 'Bulk measurement of gas content'); the value thereby obtained  $-39.0 \text{ m}^{-1}$ —gave a porosity of 97.6%. A visual inspection of the 3D CT image showed that this mid-point threshold overestimates the bulk porosity; reducing the threshold linear attenuation below  $39.9 \text{ m}^{-1}$  increases the size of the *Sphagnum* stems and branches without introducing a significant number of apparently erroneously classified voxels that do not conform to the expected peat structure. The approach overestimates the bulk porosity because the standard deviations of the *Sphagnum* and water peaks are not equal (Figure 8). The *Sphagnum* peak has a higher standard deviation because the lead sorption varies spatially. To account for the variability in the standard deviation between the water and *Sphagnum* peaks, a new threshold attenuation was applied. This threshold of  $34.4 \text{ m}^{-1}$  equals the intercept between the water and *Sphagnum* normal distributions (Figure 8). This threshold was validated from a visual inspection of the classified image and gives a bulk porosity of 95.7%. Although the *Sphagnum* leaves are not identifiable within this classified image, the resultant error in the measured porosity will be small because chlorophyllose cells with *Sphagnum* leaves comprise only a very small proportion of the sample volume. However, it should be noted that the threshold approach will slightly underestimate the actual porosity.

#### Quantification of peat structure

While the CT approach may be applied to measure widely used bulk hydrological parameters, the high resolution spatial nature of the measurements provides far more detailed information about the peat structure. Such information includes, for example, the length of the

*Sphagnum* branches and stems, their radius and their orientation. However, the presentation of measurements in raster form (as above) makes such analysis of the peat structure difficult. Consequently, the data set was vectorised using the skeletonisation process of Fouard *et al.* (2006). First, the *Sphagnum* stems and branches are classified using the threshold approach discussed above. Note that, if only information on the structure of the stems is required, the threshold can be altered to remove the branches from the classified image (Figure 7a). The skeletonisation process then calculates the shortest distance from each voxel that has been classified as *Sphagnum* to a voxel classified as water. This 'distance map' is thinned to produce a single line of voxels through the centre of the *Sphagnum* stems and branches. A 'centre line' is then drawn through these voxels and stored as Cartesian coordinates. The value of each voxel in the distance map through which the centre line is drawn is also stored. This is equal to the radius of the stem or branch at that location. A 3D representation of the vector data set is presented in Figure 9. A movie image of this data set is also available in the 'supporting information'. In this movie file, the colour of the centre line is dependent on the radius of the stem or branch. The *Sphagnum* stems are identifiable as having the greatest radius and

are represented by the yellow line. The branches, of a smaller radius, are shown in blue.

The vectorised image can be analysed to obtain any required metrics of the structure of the *Sphagnum* peat, as demonstrated by the following simple examples. Each vector was classified as a *Sphagnum* stem, branch or unconnected length. A *Sphagnum* stem is defined as a vector which is connected at both ends to other vectors. The length of all the *Sphagnum* stems in the vectorised image totalled 1.82 m, with an average radius of 0.65 mm. A *Sphagnum* branch is defined as a vector that is not connected at one end, but connected to other vectors at the other end. There were 1309 *Sphagnum* branches in the sample. Each branch averages 3.2 mm in length, with an average radius of 0.23 mm. The physical measurements of branch lengths of a separate sample of *S. magellanicum* suggests that this may be an underestimation (average branch lengths = 5.7 mm,  $n = 30$ , st. dev = 0.8 mm). This could result from (i) the classification of the CT image not capturing the ends of the branches, and (ii) the division of some branches into two vectors part way along their length (e.g. branch A and B; Figure 9). Such divisions will, on average, reduce the measured branch length by a third. Excluding branches below a threshold length (Fouard *et al.*, 2006) and applying a more sophisticated classification of *Sphagnum* branches, grouping divisions that do occur into a single branch, would overcome this current limitation.

The average vertical orientation of each *Sphagnum* stem and branch was also calculated (Figure 10). The *Sphagnum* stems and branches are both preferentially orientated in the horizontal direction, with average angles from the horizontal of 30.2° (st. dev 19.7) and 32.3° (st. dev 21.3), respectively. An unconnected length is defined as a vector that is not connected at either end. The unconnected lengths are located predominantly around the outside of the sample. These result from the sample being trimmed to the correct dimensions prior to scanning. Individual *Sphagnum* plants were also identified; they are defined as a group of interconnected stems and branches. For example, the stem length of *Sphagnum* plant number 13 was 73.6 mm long with 61

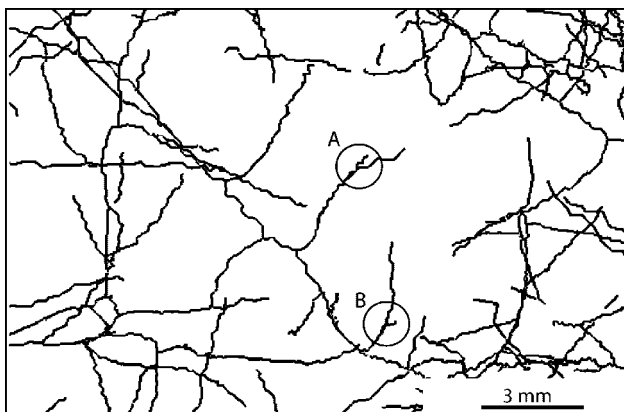


Figure 9. Vectorised image of the *S. magellanicum* stems and branches. Circles A and B mark examples of where the vectorised *Sphagnum* branches divide part way along into two vectors. This division causes the first section of the branch to be erroneously classified as a stem in the subsequent data processing

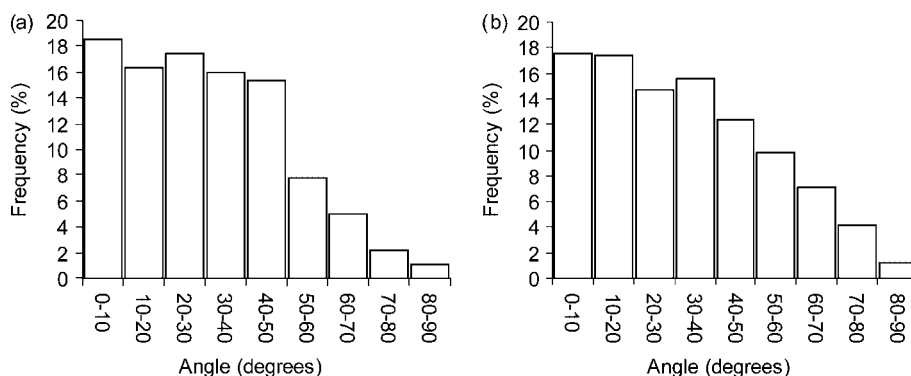


Figure 10. Angle of (a) *Sphagnum* stems and (b) *Sphagnum* branches from the horizontal calculated from the vectorised image of the *S. magellanicum* stems and branches

branches. However, overlap between differing *Sphagnum* plants made their exact identification difficult. For example, *Sphagnum* plant 6 was 1.12 m in length with 738 branches. These unrealistically long plant remains result from interconnected branches being mistaken as stems, grouping different *Sphagnum* plants together. This may be overcome by combining vectorised images of *Sphagnum* stems obtained at one threshold (Figure 7a), with vectorised *Sphagnum* branches obtained at a second threshold (Figure 7b). Alternatively, the average radius of each vector may be used to classify it as either a stem or a branch.

## CONCLUDING REMARKS

### *Biogenic gas bubbles*

Entrapped gas bubbles have been identified from a CT scan of a sample of *Sphagnum* peat. Two approaches to calculating the bulk gas content of the peat have been presented. Fitting normal distribution curves to the linear attenuation histogram is considered to provide the most accurate measurement. However, spatial variations in the gas content within the sample cannot be analysed because individual voxels are not classified as either gas or water. The second method, the threshold approach, provides similar measurements of the bulk gas content of the peat and classifies each voxel as either gas or water.

Individual gas bubbles were identified by grouping together neighbouring gas voxels. Basic characteristics of these gas bubbles (size, location and shape) have been analysed, to show the potential of the CT approach. However, the possible future applications are extensive. Gas bubbles can be identified without any preparation of the sample, making the measurement approach non-destructive. A sample of peat can be scanned on multiple occasions without influencing the physical processes. Therefore, CT scans may, for example, be performed before and after a hydraulic gradient has been applied across a sample to identify the mobility and coalescence of biogenic gas bubbles. However, the effect of the radiation dose on the microbiological processes is currently unclear. Further work is therefore required to identify whether peat samples can be scanned during incubations, to investigate the development and ebullition of biogenic gas bubbles, without affecting methane production. Performing scans before and after ebullition events could be used to investigate the loss of individual gas bubbles from the peat. If the microbiological processes are sensitive to the applied radiation dose, this could be overcome by doping the sample with fresh methanogens between scans. While this would restrict conclusions about the volumes of biogenic gas produced during incubations, such an approach would still provide process information concerning the development and ebullition of biogenic gas bubbles.

### *Peat structure*

The linear attenuations of peat and water have been shown to be indistinguishable within CT scans, even

with the application of dual energy CT. Peat samples must therefore be prepared prior to scanning. Flushing the peat with lead (II) nitrate was the most successful approach, since *Sphagnum* stems and branches were clearly identifiable in the resultant CT image. However, *Sphagnum* leaves cannot be identified because they are composed predominantly of water-filled hyaline cells. While the inability of the CT approach to identify *Sphagnum* stems will have only a minimal influence on the measured porosities, the leaf distribution may be important when considering processes occurring within the peat profile. Notably, the leaf distribution may act as an important property of the peat, responsible for entrapping of small gas bubbles. However, the inability of the CT approach to identify *Sphagnum* leaves may not be very critical as leaf distribution is probably related to the distribution of branches and stems within the peat profile.

Skeletonisation of the raster CT image produced a vectorised image of the peat structure that was analysed to produce quantitative measurements of the peat structure. Simple characteristics of the peat were analysed—including the length of the *Sphagnum* stems, the number of branches and their orientation—demonstrating the potential of the approach. These metrics can be applied as an indicator of peat decay (Johnson *et al.*, 1990), hydraulic conductivity, or the ability of the peat to retain biogenic gas bubbles.

### *Future development of CT scanners*

The X-ray computed tomography approach has shown great potential for the study of peat soils; in measuring the physical properties of entrapped gas bubbles and quantifying the structural properties of the peat. However, the study of peat samples using microCT scanners, such as that used within this study, is limited by the maximum sample sizes that can be scanned (*c.* 0.25 L). Ultimately, it would be useful to scan much larger samples (*c.* 10 L) with the same high resolution. This is because laboratory studies, for example of biogenic gas bubble development in peat, normally occur at a larger scale than this study (Baird *et al.*, 2004; Kellner *et al.*, 2006). Although traditional medical CT scanners (designed for full body scans) do enable measurements of larger samples (*c.* 10 L), they produce images of a lower resolution than microCT scanners, preventing detailed analysis of small entrapped gas bubbles and the quantification of peat structure. However, a new generation of medical scanners, which can scan large sample sizes at the same resolution as traditional microCT scanners, are becoming more widely available.

## ACKNOWLEDGEMENTS

The authors would like to thank A. Baird and A. Papadopoulos and two anonymous reviewers for their comments on a previous draft of this manuscript. The

Royal Society for the Protection of Birds, Scottish Natural Heritage and the Countryside Council for Wales all kindly provided access to the field sites.

## REFERENCES

- Baird AJ, Waldron S. 2003. Shallow horizontal groundwater flow in peatlands is reduced by bacteriogenic gas production. *Geophysical Research Letters* **30**: 2043.
- Baird AJ, Beckwith CW, Waldron S, Waddington JM. 2004. Ebullition of methane-containing gas bubbles from near surface *Sphagnum* peat. *Geophysical Research Letters* **31**: L21505.
- Beckwith CW, Baird AJ. 2001. Effect of biogenic gas bubble on water flow through poorly decomposed blanket peat. *Water Resources Research* **37**: 551–558.
- Belyea LR, Baird AJ. 2006. Beyond the “limits to peat bog growth”: cross-scale feedback in peatland development. *Ecological Monographs* **76**(3): 299–322.
- Blais KE. 2005. *Measurement of physical and hydraulic properties of organic soil using computed tomographic imagery*. Unpublished Masters of Science Thesis, Simon Fraser University.
- Clapham AR. 1936. Over-dispersion in grassland communities and the use of statistical methods in plant ecology. *The Journal of Ecology* **24**: 232–251.
- Clausnitzer V, Hopmans J. 2000. Pore-scale measurements of solute breakthrough using microfocuss X-ray computed tomography. *Water Resources Research* **36**(8): 2067–2079.
- Daulat WE, Clymo RS. 1998. Effects of temperature and watertable on the efflux of methane from peatland surface cores. *Atmospheric Environment* **32**: 3207–3218.
- Fouard C, Malandain G, Prohaska S, Westerhoff M. 2006. Blockwise processing applied to brain microvascular network study. *IEEE Transactions on Medical Imaging* **25**(10): 1319–1328.
- Gafni A. 1986. *Field tracing approach to determine flow velocity and hydraulic conductivity in saturated peat soils*. Unpublished PhD thesis, University of Minnesota, St Paul.
- Glaser PH, Chanton JP, Morin P, Rosenberry DO, Siegel DI, Ruud O, Chasar LI, Reeve AS. 2004. Surface deformations as indicators of deep ebullition fluxes in a large northern peatland. *Global Biogeochemical Cycles* **18**: GB1003.
- Greig-Smith P. 1952. The use of random and contiguous quadrates in the study of the structure of plant communities. *Annals of Botany* **16**: 293–316.
- Ho S, McKay G. 1999. Batch lead(II) removal from aqueous solution by peat: equilibrium and kinetics. *Institution of Chemical Engineers* **77**: 165–173.
- Hopkins B, Skellam JG. 1954. A new method for determining the type of distribution of plant individuals. *Annals of Botany* **18**: 213–227.
- Ingram HAP. 1978. Soil layers in mires: function and terminology. *Journal of Soil Science* **29**: 224–227.
- Johnson LC, Damman AWH, Malmer N. 1990. *Sphagnum* macrostructure as an indicator of decay and compaction in peat cores from an ombrotrophic south Swedish peat-bog. *Journal of Ecology* **78**: 633–647.
- Kellner E, Waddington JM, Price JS. 2005. Dynamics of biogenic gas bubble in peat: Potential effects on water storage and peat deformation. *Water Resources Research* **41**: W08417.
- Kellner E, Baird AJ, Oosterwoud M, Harrison K, Waddington JM. 2006. The effect of atmospheric pressure and temperature on methane (CH<sub>4</sub>) ebullition from near-surface peats. *Geophysical Research Letters* **33**(18): L18405.
- Ketcham RA, Carlson WD. 2001. Acquisition, optimization and interpretation of X-ray computed tomographic imagery: applications to the geosciences. *Computers and Geosciences* **27**: 381–400.
- Maltby E, Proctor MCF. 1996. Peatlands: their nature and role in the biosphere. In *Global Peat Resources*, Lappalainen E (ed). International Peat Society; 11–19.
- Price JS, Cagampan J, Kellner E. 2005. Assessment of peat compressibility: is there an easy way? *Hydrological Processes* **19**(17): 3469–3475.
- Rosenberry DO, Glaser PH, Siegel DI, Weeks EP. 2003. Use of hydraulic head to estimate volumetric gas content and ebullition flux in northern peatlands. *Water Resources Research* **39**(3): 1066.
- Rydin H, Jeglum JK. 2006. *The Biology of Peatlands*. Oxford University Press: Oxford.
- Strack M, Kellner E, Waddington JM. 2005. Dynamics of biogenic gas bubbles in peat and their effects on peatland biogeochemistry. *Global Biogeochemical Cycles* **19**: GB1003.
- Strack M, Kellner E, Waddington JM. 2006. Effect of entrapped gas on peatland surface level fluctuations. *Hydrological Processes* **20**: 3611–3622.
- Tokida T, Miyaxaki T, Mizoguchi M, Nagata O, Takakai F, Kagemoto A, Hatano R. 2007. Falling atmospheric pressure as a trigger for methane ebullition from peatland. *Global Biogeochemical Cycles* **21**(2): GB2003.
- Vinegar HJ, Wellington SL. 1987. Tomographic imaging of three-phase flow experiments. *Review of Scientific Instrumentation* **58**(1): 96–107.
- Wildenschild D, Hopmans JW, Vaz CMP, Rivers ML, Rikard D, Christensen BSB. 2002. Using X-ray computed tomography in hydrology: systems, resolutions, and limitations. *Journal of Hydrology* **267**: 285–297.